1   # Multimodal CEA-targeted image-guided colorectal cancer surgery

2   # using ^{111}In-labeled SGM-101

3   Jan Marie de Gooyer[1, 2], Fortuné M. K. Elekonawo[1, 2], Desirée L. Bos[1], Rachel S. van

4   der Post[3], André Pèlegrin[4], Bérénice Framery[5], Françoise Cailler[5], Alexander L.

5   Vahrmeijer[6], Johannes H. W. de Wilt[2], Mark Rijpkema[1]

6   [1]*Radboud university medical center, department of Radiology, Nuclear Medicine & Anatomy, Nijmegen, the*

7   *Netherlands.* [2]*Radboud university medical center, department of Surgical oncology, Nijmegen, the Netherlands.*

8   [3]*Radboud university medical center, department of Pathology, Nijmegen, the Netherlands.* [4] *IRCM, Institut de*

9   *Recherche en Cancérologie de Montpellier, INSERM U1194, Université de Montpellier, Institut régional du*

10   *Cancer de Montpellier, Montpellier, F-34298, France.* [5]*SurgiMab, Montpellier, France.* [6]*Leiden university medical*

11   *center, department of Surgery, Leiden, the Netherlands.*

12   **Running title:** Multimodal image-guided colorectal cancer surgery

13   **Key words:** Colorectal cancer, Image guided surgery, fluorescence imaging, preoperative imaging,

14   multi-modal imaging

15   **Corresponding author**

16   Jan-Marie de Gooyer

17   Radboudumc, Geert Grooteplein Zuid 10

18   6525 GA Nijmegen

19   +31 (0)24 366 72 44

20   jan-marie.gooyer@radboudumc.nl

21   **Disclosure statement**

22   FC and BF are employed by Surgimab, and are inventors on the patent that protects SGM-101. FC, BF

23   and AP are stockholders of Surgimab. All other authors declare no competing interests.

24

Translandslational relevance statement

With surgical procedures for colorectal cancer becoming more complicated and extensive, adequate localization and delineation of tumors can be arduous for surgeons. Intraoperative dual-modality image guided surgery with multimodal tracers is a powerful technique that may provide essential information about tumor margins and the location of metastatic lesions. In the current study, we report on the synthesis, *in vitro* characterization, *in vivo* testing and translational evaluation of a novel multimodal CEA-targeting tracer for image guided colorectal cancer surgery. SPECT/CT and fluorescence imaging clearly visualized specific tracer uptake in a colorectal peritoneal carcinomatosis model, which was confirmed by immunohistochemical analysis and gamma counting. The translational *ex vivo* incubation study with fresh surgically derived human peritoneal colorectal cancer deposits showed high tumor to background ratios of the fluorescence and radiosignal. These results demonstrate the clinical potential our multimodal CEA-targeting tracer for image guided surgery and facilitate rapid clinical implementation, which is currently in progress.

Abstract

Purpose: Intraoperative image guidance may aid in clinical decision making during surgical treatment of colorectal cancer. We developed the dual-labeled CEA-targeting tracer [111In]In-DTPA-SGM-101 for pre- and intraoperative imaging of colorectal cancer. Subsequently we investigated the tracer in preclinical biodistribution and multimodal image-guided surgery studies, and assessed the clinical feasibility on patient derived colorectal cancer samples, paving the way for rapid clinical translation.

Experimental design: SGM-101 was conjugated with p-isothiocyanatobenzyl (ITC)-diethylenetriaminepentaacetic acid (DTPA) and labeled with 111In. The biodistribution of 3, 10, 30, and 100 µg [111In]In-DTPA-SGM-101 was assessed in a dose escalation study in BALB/c nude mice with subcutaneous LS174T human colonic tumors followed by a study to determine the optimal time point for imaging. Mice with intraperitoneal LS174T tumors underwent microSPECT/CT imaging and fluorescence image-guided resection. In a final translational experiment, we incubated freshly resected human tumor specimens with the tracer and assessed the tumor-to-adjacent tissue ratio of both signals.

Results: The optimal protein dose of [111In]In-DTPA-SGM-101 was 30 µg (tumor-to-blood ratio 5.8 ± 1.1) and the optimal timepoint for imaging was 72 hours after injection (tumor-to-blood ratio 5.1 ± 1.0). In mice with intraperitoneal tumors, [111In]In-DTPA-SGM-101 enabled preoperative SPECT/CT imaging and fluorescence image-guided resection. After incubation of human tumor samples overall fluorescence and radiosignal intensities were higher in tumor areas compared to adjacent non-tumor tissue($p < 0.001$).

Conclusions: [111In]In-DTPA-SGM-101 showed specific accumulation in colorectal tumors, and enabled micro-SPECT/CT imaging and fluorescence-guided tumor resection. Thus, [111In]In-DTPA-SGM-101 could be a valuable tool for preoperative SPECT/CT imaging and intraoperative radioguided localization and fluorescence-guided resection of colorectal cancer.

74   **Introduction**

75   Colorectal cancer is currently the second leading cause of cancer death in women, and the third most

76   common cause in men(1). While therapeutic strategies have evolved throughout the last decades,

77   radical surgical resection of all tumor tissue with clear margins (R0) remains the mainstay of

78   treatment. Surgical treatment has become increasingly versatile with procedures such as

79   cytoreductive surgery for colorectal peritoneal metastasis, or extensive exenterative surgery for

80   locally advanced or recurrent rectal cancer(2, 3). Complete tumor resection is pivotal for successful

81   treatment outcome, but remains challenging in many patients. In rectal cancer, involvement of the

82   circumferential resection margin (CRM) still occurs in 1 to 28% of all surgically treated cases(4). There

83   are several factors that can complicate surgical treatment, such as distorted pelvic anatomy after

84   previous resections, multifocal tumor deposits, the presence of multiple small tumor nodules in

85   peritoneally metastasized cancers, and difficulty to distinguish benign from malignant tissue, for

86   example after neo-adjuvant therapy(5). Real-time intraoperative margin assessment and tumor

87   visualization techniques guiding the surgeon may be advantageous to overcome these obstacles.

88

89   Carcinoembryonic antigen(CEA)-targeted fluorescence imaging is a technique that can be of added

90   value in surgical treatment of both locoregional and metastasized colorectal cancer. CEA is a widely

91   known glycoprotein and tumor marker that is highly expressed on almost all (more than 95%)

92   colorectal cancers, but also on a variety of other malignancies such as gastric, pancreatic, lung, breast

93   and esophageal cancer(6). SGM-101 is a CEA-specific chimeric antibody conjugated to a near-infrared

94   fluorophore that has been developed to facilitate CEA-targeted fluorescence image-guided surgery of

95   colorectal cancer(7).

96   Preclinical toxicology, pharmacology and pharmacokinetic results have demonstrated the absence of

97   significant adverse effects of SGM-101 at doses well above the anticipated maximal human exposure

98   (8). A previous phase I/II clinical trial has also already shown the potential of SGM-101 for

99   intraoperative detection of colorectal cancer tissue. In this trial, CEA-targeted fluorescence-guided

100   surgery resulted in the detection of additional malignant lesions that were not clinically suspect,

101   emphasizing the potential of SGM-101 for intraoperative tumor detection of colorectal cancer(9).

102

103   While the use of targeted near-infrared fluorescence-guided surgery is of great value to enhance

104   oncological procedures, the limited tissue penetration depth of NIR-fluorescent light confines

105   application to superficial tumors. Accurate visualization of deeper located tumors is difficult and only

106   feasible after proper surgical exposure(9). Adding a radiolabel to a fluorescent tumor-targeting tracer

107   may overcome this limitation by facilitating intraoperative radioguidance(10). Such a dual-labeled

108   tracer also enables preoperative imaging with SPECT/CT and straightforward quantification in

109   (pre)clinical research by gamma counting(11). Quantitative assessment of tracer accumulation and

110   subsequent determination of the tumor to background ratio is a key determining factor of tumor

111   detectability and sensitivity of the imaging technique, but accurate quantification of NIR-

112   fluorescence is difficult and reported values differ widely(12). Thus, a tracer containing both a

113   fluorophore and a gamma radiation emitting radionuclide may be a powerful approach(13).

114

115   In this study, SGM-101 was conjugated to a radiolabel (^{111}In) to create the dual-labeled tracer

116   [^{111}In]In-DTPA-SGM-101. We evaluated the characteristics, immunoreactivity and stability of this new

117   tracer in vitro. Subsequently we determined the in vivo biodistribution, and performed CEA-targeted

118   micro-SPECT and fluorescence image-guided surgery in a CEA-expressing colorectal cancer xenograft

119   model. In a final translational experiment, we investigated this new tracer in an ex vivo incubation

120   experiment with patient derived surgically resected peritoneal colorectal cancer deposits.

121

122

123

124 **Materials & Methods**

125 *Synthesis of DTPA-SGM-101*

126 SGM-101 is a highly specific anti-CEA chimeric monoclonal antibody(ch511) conjugated to a

127 fluorophore in the 700 nm range (BM104). Clinical grade SGM-101 was obtained from Surgimab

128 (Montpellier, France)(7). First, SGM-101 was dialyzed for 5 days in a Slide-A-Lyzer (10-kDa cutoff;

129 Pierce Biotechnology Inc, Waltham, MA, USA.) against a 0.5M phosphate-buffered saline (PBS)

130 solution. Subsequently, SCN-Bz-DTPA (Macrocyclics, Plano, TX, USA) was added in a 3-fold molar

131 excess in Dimethyl sulfoxide (DMSO). After 1 hour of incubation at room temperature on an orbital

132 shaker in the dark, the reaction mixture was dialyzed for 5 days in a Slide-A-Lyzer (10-kDa cutoff;

133 Pierce Biotechnology Inc, Waltham, MA, USA.). against PBS. The final concentration of the new

134 conjugate was determined spectrophotometrically at 280 nm using an Infinite M200 Pro multimode

135 reader (Tecan group Ltd, Männedorf, Switzerland). The optical properties of both the SGM-101

136 starting material and the new conjugate were investigated. Absorbance and fluorescence spectra of

137 both solutions were determined using the Infinite M200 Pro multimode reader. A radiolabeling of

138 the new DTPA-SGM-101 with Indium-111 was done (see below) before and after dialysis to calculate

139 the conjugation ratio of the chelator DTPA to SGM-101. HPLC analysis of the radiolabeled conjugate

140 was performed to determine the radiochemical purity of the new compound.

141

142 *Radiolabeling and Quality Control of DTPA-SGM-101*

143 For the first 2 biodistribution experiments on mice with subcutaneous tumors, DTPA-SGM-101 was

144 labelled with 0.5 MBq of ^{111}In (Curium, Petten, the Netherlands) in 0.5M 2-(N-morpholino)

145 ethanesulfonic acid (MES) buffer, pH 5.4 (2 times the volume of the [^{111}In]InCl$_3$ solution), and

146 incubated for 20 min at room temperature under metal-free conditions. For studies where SPECT/CT

147 was performed, DTPA-SGM-101 was radiolabeled with 10 MBq of ^{111}In per mice under similar

148 conditions. Subsequently, 50 ethylenediamine tetraacetic acid (EDTA) solution was added (final

149 concentration, 5 mM) to chelate unincorporated ^{111}In. Final labelling efficiency of the compound was

150   determined by instant thin-layer chromatography on silica gel strips (Agilent Technologies,

151   Amstelveen, The Netherlands), where a 0.15 M citrate buffer with pH 6.0 was used as mobile phase.

152   The labelling efficiency exceeded 98% for all experiments.

153   The immunoreactivity of [^{111}In]In-DTPA-SGM-101 was determined with LS174T cells , as described by

154   Lindmo et al[14]. In short: A serial dilution of LS174T cells was incubated with [^{111}In]In-DTPA-SGM-

155   101 for 30 min at 37°C. Subsequently, cells were centrifuged and analyzed in a shielded 3"-well-type

156   γ-counter (Perkin-Elmer, Boston, MA, USA). The LS174T colorectal cancer cells used in all

157   experiments were originally acquired from the American Type Culture Collection (ATCC, Manassas,

158   VA, USA, Batch F-9126). Cells were last tested for *Myxoplasma* in January 2018. All experiments

159   were conducted within 1 to 2 months after thawing.

160   *Tumor models*

161   All animal experiments were conducted with 6- to 8-week-old female athymic BALB/c nu/nu mice

162   (Janvier, Le Genest-Saint-Isle, France) weighing 20–25 g. Mice were given at least 1 week to become

163   accustomed to laboratory conditions before starting with the experiments. Mice were housed in

164   individually ventilated filter topped cages under nonsterile standard conditions with free access to

165   chlorophyll free chow and water in accordance with institutional guidelines. The subcutaneous

166   tumors were induced by subcutaneous injection of 3 x 10^5 LS174T cells in 200 µL of RPMI 1640

167   medium (Gibco, Thermo Fischer Scientific, Waltham, MA, USA) in the right flank of the mice.

168   Intraperitoneal tumors were induced as described previously by Koppe et al[15]. In summary, mice

169   were injected intraperitoneally with 10^6 LS174T cells suspended in 300 µL of RPMI 1640 medium.

170   Experiments were continued 1-2 weeks after tumor cell injection.

171

172   *SPECT/CT and Fluorescence imaging*

173   SPECT/CT and fluorescence imaging was performed as described previously by Rijpkema et al[16]. In

174   summary, SPECT/CT images were acquired with the U-SPECT-IICT system (MILabs, Utrecht, the

175   Netherlands). Mice were imaged for 2 frames of 25 minutes using a 1.0-mm-diameter pinhole

176   collimator, followed by a CT scan for anatomic referencing (spatial resolution 160 μm; 65 kV; 612

177   μA). All scans were reconstructed with software supplied by MILabs, using an ordered subset

178   expectation maximization algorithm with a voxel size of 0.375 mm. SPECT/CT images were

179   subsequently analyzed and created using the Inveon Research Workplace Software (IRW, version

180   4.1). Fluorescence images were acquired with an in vivo imaging system (Xenogen VivoVision IVIS

181   Lumina II; Caliper Life Sciences, Hopkinton, MA, US). The acquisition time was 1–2 min with the

182   following parameters: F/stop 2; binning medium; field of view C; excitation filter 605 nm; emission

183   filter 695-770 nm. Correction for autofluorescence was performed using a second acquisition of 10 s

184   with an excitation filter of 605 nm.

185

186   *Immunohistochemistry*

187   Immunohistochemistry was performed as described by Elekonawo et al (17). Slides were

188   deparaffinized with xylene, rehydrated in ethanol and rinsed in distilled water according to standard

189   local protocol. Heat-induced antigen retrieval was performed in EDTA solution (pH 9.0). Endogenous

190   peroxidase activity was blocked with 3% H_2O_2 in 10 Mm PBS for 10 minutes at room temperature.

191   Subsequently, tissue sections were washed with 10 mM PBS and stained with primary antibodies

192   (CEA: Mouse monoclonal; Clone COL-1; MS-613-P; Neomarkers Fremont, CA, USA). Next, sections

193   were incubated with biotin free Poly-HRP-anti mouse/rabbit IgG (ImmunoLogic/VWR International

194   B.V., Amsterdam, The Netherlands) in EnVision™ FLEX Wash Buffer (Dako Denmark A/S, Glostrup,

195   Denmark) (1:1) at room temperature for 30 minutes. Antibody binding was visualized using the

196   EnVision™ FLEX Working Solution (Dako Denmark A/S, Glostrup, Denmark) at room temperature for

197   10 minutes. All sections were counterstained with hematoxylin for 5 seconds and subsequently

198   dehydrated in ethanol and coverslipped.

199

200 *Ethical Approval*

201 All animal experiments were approved by the Animal Welfare Committee of the Radboud University

202 Medical Center (Local code: 2015-0071-147) and were conducted in accordance with the Revised

203 Dutch Act on Animal Experimentation (Wet op de Dierproeven). The experiments involving the use of

204 surgically derived human tissue samples have been carried out according to the principles of the

205 Declaration of Helsinki. The study protocol and collection of tissue were approved by the research

206 ethics committee of the region Arnhem-Nijmegen (CMO regio Arnhem-Nijmegen, file code 2019-

207 5437).

208

209 *In Vivo Experiments*

210 *Dose escalation study*

211 Mice with subcutaneous LS174T tumors on their right flank received an intravenous injection of 3,

212 10, 30, or 100 μg of $[^{111}In]$In-DTPA-SGM-101 per mouse (5 mice per group). A 5th group received 30

213 μg of radiolabeled $[^{111}In]$In-DTPA-SGM-101 complemented with 1 mg of unlabeled DTPA-SGM-101 as

214 control group. Three days after injection of $[^{111}In]$In-DTPA-SGM-101 , mice were euthanized using

215 O_2/CO_2 asphyxiation and blood, lung, heart, spleen, pancreas, stomach, small intestine, kidney, liver,

216 muscle and tumor were dissected and weighed. Activity in all resected specimens was measured in a

217 gamma-counter (2480 WIZARD2; PerkinElmer). To calculate the uptake of radiolabeled antibodies in

218 each sample as a fraction of the injected activity, aliquots of the injected dose were counted

219 simultaneously. The results were expressed as percentage injected activity per gram (%IA/g).

220

221 *Optimal time point determination*

222 Mice with subcutaneous LS174T tumors received the optimal protein dose of 30 μg (as determined in

223 the previous dose escalation study) of $[^{111}In]$In-DTPA-SGM-101 (10 MBq per mouse). After 24, 48, or

224 72 hours (5 mice at each time point), SPECT/CT and fluorescence imaging was performed as

225 described above. Subsequently, mice were euthanized and the biodistribution of the radiolabel was

226   determined as described in the previous experiment to assess the optimal timepoint for imaging

227   after administration of the dual-labeled tracer.

228

229   *Preoperative SPECT and fluorescence image–guided surgery study*

230   Using the optimal conditions as determined in the first two in vivo studies, multimodal image-guided

231   surgery was performed in mice with intraperitoneally growing LS174T tumors as previously described

232   by Rijpkema et al (16). Mice received 30 µg of [^{111}In]In-DTPA-SGM-101 (10 MBq per mouse; 4 mice) or

233   30 µg of [^{111}In]In-DTPA-SGM-101 (10MBq per mouse, 2 mice) with 1 mg of unlabeled DTPA-SGM-101

234   that served as a negative control. Three days after administration of the antibody conjugate,

235   preoperative SPECT/CT images were acquired, followed by fluorescence imaging (as described above)

236   of the mice in supine position after surgical relocation of skin, abdominal muscle layers, and

237   peritoneum. Subsequently, the visualized tumor nodules were resected and fluorescence imaging

238   was repeated to check for residual tumor tissue. This procedure was repeated until all tumor nodules

239   were removed.

240   *Ex vivo incubation of fresh patient-derived peritoneal tumor samples*

241   Finally, a translational experiment was conducted to assess tumor to surrounding (normal) tissue

242   contrast in human tissue samples using fluorescence imaging and autoradiography as previously

243   described by Elekonawo et al(17). Fresh surgically obtained peritoneal colorectal cancer deposits

244   were incubated in tissue culture medium containing the tracer [^{111}In]In-DTPA-SGM-101. Immediately

245   after surgical resection, colorectal peritoneal tumor deposits were acquired and subsequently

246   incubated overnight at 37°C in DMEM supplemented with 1% penicillin/streptomycin and 0.1%

247   bovine serum albumin (BSA)(Sigma-Aldrich Chemie N.V., Zwijndrecht, Netherlands) and 4 µg·ml^{-1},

248   [^{111}In]In-DTPA-SGM-101 (0.05 MBg/ug). After incubation overnight, tumor deposits were washed in

249   at least 3L of continuously moving serially refreshed phosphate-buffered saline supplemented with

250   0.1% BSA at 4-8°C for a minimum of 6 hours. Specimens were subsequently fixed in formalin and

251   embedded in paraffin. Four μm tissue sections were cut and placed on glass slides. Fluorescence

252   images were acquired on a closed field fluorescence imaging system (Odyssey CLx; LI-COR

253   Biosciences, Lincoln, NE, USA). Slides were then placed on a photostimulable phosphor plate. After 7

254   days, we imaged the plate on a phosphor imager (Typhoon FLA 7000 phosphor imager, GE

255   Healthcare, Hoevelaken, The Netherlands) Subsequently slides were stained with eosin &

256   haematoxylin (H&E) and immunohistochemistry (IHC) of carcinoembryonic antigen (CEA)(mouse

257   monoclonal; Clone COL-1; MS-613-P; Neomarkers Fremont, CA, USA) was performed. Surgical

258   specimens from two patients received a non-specific hIgG antibody-conjugate (SouthernBiotech,

259   Birmingham, AL, USA) as negative controls. An independent pathologist reviewed the H&E and CEA

260   slides to verify the presence and location of tumor cells. Regions of interest (ROI) (tumor and

261   adjacent normal tissue) were drawn in the corresponding fluorescence and autoradiography images

262   to determine tumor to background ratios of both fluorescence and radiosignal.

263   *Statistical analysis*

264   Statistical analyses were performed using SPSS Statistics 25.0 (IBM) and GraphPad Prism software

265   (version 5.03; GraphPad Software). Tissue uptake at the different protein dose levels and time points

266   was tested for significance using a 1-way ANOVA test with post hoc Bonferroni correction. To test for

267   differences in tumor and normal fluorescence and autoradiography intensities, a Mann-Whitney U

268   test was used. Mean tumor to background ratios of the experimental group were compared to mean

269   tumor to background ratios in the control groups with an independent samples t-test. An α-value <

270   0.05 was considered to be statistically significant in all analyses.

271

272   **Results**

273   Comparison of SGM-101 and DTPA-SGM-101 showed similar patterns of absorbance and

274   fluorescence emission before and after conjugation to the chelator (supplemental figure 1). The

275   substitution ratio of SGM-101 and DTPA was 1. The immunoreactive fraction of all conjugates

276   exceeded 80% and radiochemical purity of [^{111}In]In-DTPA-SGM-101 used in all studies was >99%.

277

278   In the dose escalation study, [^{111}In]In-DTPA-SGM-101 specifically accumulated in the subcutaneous

279   CEA-positive LS174T tumors, with mean tumor uptake of 56.3 ± 14.2, 42.5 ± 15.1, 46.2 ± 6.7 and 21 ±

280   1 %IA/g after injection of 3, 10, 30 and 100 μg, respectively. Tumor to blood ratios of mice that were

281   injected with 3, 10, 30 or 100 μg were 5.6 ± 1.3, 5.0 ± 0.9, 5.8 ± 1.1 and 2.3 ± 0.4, respectively. Adding

282   an excess of 1 mg unlabeled DTPA-SGM-101 decreased tumor uptake to 5.3 ± 0.4 %IA/g and the

283   tumor-to-blood ratio to 0.53 ± 0.2 %IA/g, illustrating that tumor uptake of [^{111}In]In-DTPA-SGM-101

284   was specific. Based on these results, 30 μg was chosen as the optimal dose for subsequent

285   experiments. Results of the biodistribution are summarized in figure 1.

286

287   In the second study, SPECT/CT imaging, NIR-fluorescence imaging and biodistribution studies were

288   performed 24, 48 and 72 hours after administration. Tumor uptake was 34.5 ± 5.4, 42.0 ± 16.1 and

289   56.4 ± 13.9 %IA/g after 24, 48 and 72 hours respectively. Tumor to blood ratios were 2.5 ± 0.5 after

290   24 hours, 3.7 ± 0.8 after 48 hours and 5.1 ± 1.0 after 72 hours. Tumors could be visualized with both

291   SPECT and fluorescence imaging at each time point. Seventy-two hours after administration of

292   [^{111}In]In-DTPA-SGM-101 was chosen as the optimal time point for the imaging of peritoneal tumors in

293   the next experiment. The results of this study determining the optimal timepoint are summarized in

294   supplemental figure 2.

295

296   In the third in vivo experiment, we performed preoperative SPECT/CT imaging and fluorescence-

297   guided resection of tumor deposits in mice with intraperitoneally growing tumors. First, SPECT/CT

298   images were acquired to visualize the extent of peritoneal disease dissemination. Subsequently mice

299   were euthanized, and laparotomy was performed to search for tumor deposits. After suspected

300   tumors were found by combining visual inspection and SPECT/CT imaging, fluorescence images were

301   acquired and tumors were resected. Figure 2 shows that after resection of all macroscopically visible

302 tumors, fluorescence imaging revealed submillimeter tumor deposits that were initially missed by

303 visual inspection. Mice that received the optimal dose with the addition of 1 mg unlabeled DTPA-

304 SGM-101 did not show any specific accumulation of the tracer in the tumor on both imaging

305 modalities (fluorescence imaging and SPECT). Immunohistochemical analysis showed clear

306 concordance between CEA-expressing tumor cells, fluorescence and radiosignal (Supplemental figure

307 3).

308 In a final translational experiment, we collected 43 peritoneal deposits from 11 patients (3 male, 8

309 female). Median age was 76 (65-78) years. Seven patients were diagnosed with a peritoneally

310 metastasized adenocarcinoma. In one patient the peritoneal metastases originated from a mucinous

311 adenocarcinoma and in another patient from a signet-ring cell carcinoma. In one case the peritoneal

312 deposits contained a low grade appendiceal mucinous neoplasm (LAMN), and one other case was an

313 epithelial ovarian cancer. These last two cases did not express CEA and were used as negative

314 controls.

315 After the incubation experiment, subsequent series of slides were produced from the surgically

316 resected tumor deposits. This resulted in 43 series of slides that were analyzed. Thirty-three of the

317 resected peritoneal deposits contained malignant cells. The other 10 lesions did not contain vital

318 malignant tumor cells and consisted of fibrosis, necrosis, mucin, stroma or fat. Median fluorescence

319 intensity was 1371 (IQR: 1020-1834) in tumors. This was significantly higher compared to adjacent

320 normal tissue (fat, peritoneum or stroma) where the median fluorescence intensity was 293 (IQR:

321 168 - 317) ($p < 0.001$). Median intensity of the autoradiography for tumor tissue was $10.46 \cdot 10^6$ (IQR:

322 $5.192 \cdot 10^6 - 14.66 \cdot 10^6$). The median autoradiography intensity in adjacent non-tumor tissue was

323 $1.913 \cdot 10^6$ (IQR: $1.142 \cdot 10^6 - 2.724 \cdot 10^6$) ($p < 0.001$). Tumor to background ratios for the fluorescence

324 and radiosignal of all cases are shown in figure 3. Fluorescent and radiosignal-based tumor to

325 background ratios are significantly lower in the CEA-negative cancers (no radiography data available

326 for the LAMN due to a technical failure)and in the control cases incubated with the aspecific hIgG (p

327 < 0.001 for both signals). Three examples of slides (H&E, CEA, fluorescence and autoradiography) are

328 provided in figure 4, illustrating the concordance between CEA-positive tumor cells and fluorescence

329 and radiosignal. Microscopic images at a higher magnification confirming colocalization of CEA-

330 expressing tumor cells and the fluorescence signal are shown in supplemental figure 4.

331 **Discussion**

332 This study shows the in vitro and in vivo characterization of [^{111}In]In-DTPA-SGM-101 and the

333 feasibility of multimodal image-guided surgery using this tracer. Accumulation of [^{111}In]In-DTPA-SGM-

334 101 was high and specific in subcutaneous and peritoneal CEA-expressing LS174T xenografts. The

335 biodistribution of this ^{111}In-labeled fluorescent tracer showed high tumor to blood ratios and low

336 uptake in other organs. Translational ex vivo incubation studies with fresh surgically derived human

337 peritoneal colorectal cancer deposits showed high tumor to background ratios and overall

338 correspondence of both the fluorescence and radiosignal, suggesting the feasibility of this tracer for

339 multimodal image-guided surgery of CEA-expressing colorectal cancer, warranting further evaluation

340 in clinical studies.

341 The biodistribution of SGM-101 has been extensively investigated by Gutowski et al. in a similar

342 colorectal cancer model(7). The reported results show a highly similar in vivo distribution of the

343 tracer, with high uptake in the tumor compared to other tissues. As expected, conjugation of DTPA to

344 SGM-101 and subsequent radiolabeling with ^{111}In did not affect the in vivo behavior and distribution

345 of SGM-101, as in accordance with the literature(18-20). The substitution ratio of DTPA to SGM-101

346 in our study was 1, which proved sufficient for radiolabeling in all experiments. Most chelating

347 molecules can be conjugated to full IgG antibodies in ratios of up to 5 without significantly

348 influencing or altering the immunoreactivity and in vivo behavior of the antibody(18-20). Since the in

349 vivo behavior of iodinated SGM-101 and [^{111}In]In-DTPA-SGM-101 is comparable, [^{111}In]In-DTPA-SGM-

350 101 could be used for quantification of tracer in tissue and blood, facilitating pharmacokinetic

351 analysis of SGM-101 in a clinical setting.

352 In addition to accurate tracer quantification and pharmacokinetic analysis, intravenous injection of

353 this dual-labeled tracer could facilitate clinical decision making by improving preoperative tumor

354 imaging. Whole body SPECT/CT imaging might be used as an additional tool for non-invasive

355 preoperative staging of the primary tumor, distant metastases and lymph node metastases in

356 colorectal cancer patients, potentially adding to improved selection of patients with peritoneal

357 metastases who are eligible for cytoreductive surgery and hyperthermic intraperitoneal

358 chemotherapy. Conventional imaging modalities tend to underestimate the degree of intraperitoneal

359 tumor extent in these patients[21]. As a result of this underestimation, surgical procedures are

360 performed on patients that are diagnosed with irresectable disease after surgical exploration of the

361 abdomen, resulting in futile laparotomies or incomplete cytoreduction[21-24]. SGM-101

362 fluorescence-guided cytoreductive surgery for colorectal peritoneal carcinomatosis has already been

363 tested in a multicenter pilot study and in one third of all cases, detection of additional malignant

364 lesions by fluorescence imaging led to an adjustment of the peritoneal carcinomatosis index (PCI)

365 [25]. Preoperative SPECT/CT imaging might also be used as a diagnostic aid to determine whether

366 patients have extra-abdominal disease. Current criteria for determining if lymph nodes or lung

367 nodules are malignant are mainly based on size and morphological features. A tumor-targeted

368 molecular imaging approach might be valuable in determining whether lymph nodes and lung

369 nodules that are considered borderline on conventional CT are malignant or benign. Combining these

370 benefits of fluorescence-guided surgery with the additional value of a radiolabel could potentially

371 improve diagnosis and treatment of these patients even further and will be evaluated in a clinical

372 trial.

373 Another potential application of preoperative SPECT/CT imaging is the evaluation of metastatic

374 lymph node status in patients with rectal cancer after preoperative radiation based treatment. The

375 current imaging modality of choice for determining the lymph node status is Magnetic Resonance

376 Imaging (MRI), but reported sensitivity is low[26]. CEA targeted preoperative SPECT/CT could

377 potentially be used as a restaging modality after neoadjuvant (chemo)radiotherapy since CEA-

378   expression is not influenced by neoadjuvant treatment(27). Subsequently, if patients exhibit tracer

379   uptake in lymph nodes outside the standard total mesorectal resection specimen, such as lateral

380   pelvic lymph nodes, radioguidance with a gamma probe could perhaps aid in localizing these lymph

381   nodes. Subsequent intraoperative real time fluorescence imaging could also help the surgeon in

382   performing a complete resection of all metastatic lymph nodes and the primary tumor.

383   Besides colorectal cancer, combined CEA-targeted radioguidance and fluorescence imaging can

384   potentially be translated to other CEA-expressing malignancies as well. De Gouw et al. have shown

385   that 68% of lymph node metastases of esophageal cancer express CEA(28). Approximately one third

386   of all surgically treated patients with esophageal cancer have lymph node metastases after

387   neoadjuvant treatment, but lymphadenectomy is always performed because adequate treatment

388   response assessment of lymph node metastases is not possible with current imaging modalities(29).

389   CEA-targeted multimodal imaging might aid in minimizing or possibly omitting this procedure and

390   reduce the associated morbidity in selected cases. The same hypothesis is worth investigating in

391   gastric cancer, where similar dilemmas exist(30). CEA-targeted multimodal imaging could be

392   investigated as a potential aid in identifying additional metastatic lymph nodes outside of the

393   standard resection plane. It might also guide the surgeon in deciding to perform a less invasive D1

394   lymph node dissection instead of the more extensive D2 dissection which is associated with

395   increased morbidity(31, 32). In pancreatic cancer, fluorescence-guided surgery with SGM-101 was

396   successful despite suboptimal intrinsic characteristics such as poor vascularization, abundant

397   presence of desmoplastic stroma and localization of solitary ducts of tumor cells within benign

398   pancreatic tissue(33). However, tumor to background ratios were lower as compared to colorectal

399   cancer(9, 33). The addition of a radiolabel could be of added value when performing CEA-targeted

400   image-guided surgery in these patients, similar to Hekman et al, who successfully translated this

401   approach of multimodal tumor-targeted image-guided surgery into the clinic(10, 34). In a first clinical

402   study they demonstrated the feasibility of combining preoperative SPECT/CT imaging, intraoperative

403   gamma probe detection and NIR-fluorescence-guided surgery in patients with clear cell renal cell

404   carcinoma(10).

405   There are some limitations to this study that have to be addressed. First, a mouse model with human

406   colorectal cancer xenografts was used and one should consider that CEA-expression may be more

407   heterogeneous in a clinical setting. Since we did not use transgenic human CEA-expressing mouse

408   models, tumor to background ratios will not be directly translatable to the clinical setting. However,

409   in the preclinical toxicology study, the biodistribution of iodinated SGM-101 did not differ

410   significantly between transgenic CEA-expressing mice and wild type animals because physiological

411   CEA-expression is exclusively located on the apical side of healthy epithelial cells, which is also the

412   case with intestinal CEA-expression in humans (8, 35). Therefore it is not accessible to circulating CEA

413   targeting molecules, as opposed to malignant colorectal tumors, where CEA is overexpressed on the

414   entire cell surface at a 60-fold higher density (35, 36). Second, the translational experiment that was

415   performed with surgically derived peritoneal tumor deposits relies on passive diffusion of the tracer

416   into the tissue to establish adequate uptake and tumor to background ratios. Since passive diffusion

417   of full IgG antibodies will only facilitate penetration of approximately 100 μm within 12 to 18 hours

418   of incubation, the center of the tumor deposit may not be reached by the tracer (17). However,

419   although tracer distribution after intravenous injection still has to be shown in the clinic, the edges

420   and invasive margins of the tumor are the main regions of interest in surgical oncology and the

421   current results show that sufficient tumor-to-background ratios were reached for both the radio- and

422   the fluorescence signal. These results are comparable to the tumor to background ratios found in the

423   clinical studies conducted with SGM-101 (9, 25, 33).

424   In conclusion, this study shows the feasibility of CEA-targeted multimodal SPECT/CT and fluorescence

425   imaging using [^{111}In]In-DTPA-SGM-101 in colorectal cancer models. [^{111}In]In-DTPA-SGM-101 enables

426   specific and sensitive detection of colorectal cancer lesions in vivo and specifically targets tumor

427   lesions in fresh surgical samples of colorectal cancer. The addition of a gamma-emitting radiolabel to

428 SGM-101 enables straightforward quantification in vivo and may facilitate preoperative detection of

429 tumors by SPECT/CT imaging. Subsequent radioguided intraoperative localization of deeper-seated

430 lesions combined with CEA-targeted fluorescence guided surgery might further benefit the surgical

431 treatment of colorectal cancer and other CEA-expressing malignancies. These promising preclinical

432 results and our experience with the fluorescent tracer in clinical trials will pave the way for rapid

433 clinical translation. Based on our results, this new multimodal tracer will likely improve clinical

434 decision making by personalized precision surgery.

435

436 **Acknowledgements**

437 The authors would like to thank Bianca Lemmers van de Weem and Karin de Haas-Cremers for the

438 assistance with the animal experiments.

439

440 *References*

441 1.   Bray F, Ferlay J, Soerjomataram I, Siegel RL, Torre LA, Jemal A. Global cancer statistics 2018:
442 GLOBOCAN estimates of incidence and mortality worldwide for 36 cancers in 185 countries. CA: a
443 cancer journal for clinicians. 2018;68(6):394-424.
444 2.   Verwaal VJ, van Ruth S, de Bree E, van Sloothen GW, van Tinteren H, Boot H, et al.
445 Randomized trial of cytoreduction and hyperthermic intraperitoneal chemotherapy versus systemic
446 chemotherapy and palliative surgery in patients with peritoneal carcinomatosis of colorectal cancer.
447 Journal of clinical oncology : official journal of the American Society of Clinical Oncology.
448 2003;21(20):3737-43.
449 3.   Brown KGM, Solomon MJ, Koh CE. Pelvic Exenteration Surgery: The Evolution of Radical
450 Surgical Techniques for Advanced and Recurrent Pelvic Malignancy. Dis Colon Rectum.
451 2017;60(7):745-54.
452 4.   Nagtegaal ID, Quirke P. What is the role for the circumferential margin in the modern
453 treatment of rectal cancer? Journal of clinical oncology : official journal of the American Society of
454 Clinical Oncology. 2008;26(2):303-12.
455 5.   Dresen RC, Kusters M, Daniels-Gooszen AW, Cappendijk VC, Nieuwenhuijzen GA, Kessels AG,
456 et al. Absence of tumor invasion into pelvic structures in locally recurrent rectal cancer: prediction
457 with preoperative MR imaging. Radiology. 2010;256(1):143-50.
458 6.   Hammarström S. The carcinoembryonic antigen (CEA) family: structures, suggested functions
459 and expression in normal and malignant tissues. Semin Cancer Biol. 1999;9(2):67-81.
460 7.   Gutowski M, Framery B, Boonstra MC, Garambois V, Quenet F, Dumas K, et al. SGM-101: An
461 innovative near-infrared dye-antibody conjugate that targets CEA for fluorescence-guided surgery.
462 Surg Oncol. 2017;26(2):153-62.

463 8.   Framery B, Gutowski M, Dumas K, Evrard A, Muller N, Dubois V, et al. Toxicity and
464 pharmacokinetic profile of SGM-101, a fluorescent anti-CEA chimeric antibody for fluorescence
465 imaging of tumors in patients. Toxicol Rep. 2019;6:409-15.
466 9.   Boogerd LSF, Hoogstins CES, Schaap DP, Kusters M, Handgraaf HJM, van der Valk MJM, et al.
467 Safety and effectiveness of SGM-101, a fluorescent antibody targeting carcinoembryonic antigen, for
468 intraoperative detection of colorectal cancer: a dose-escalation pilot study. The lancet
469 Gastroenterology & hepatology. 2018;3(3):181-91.
470 10.   Hekman MC, Rijpkema M, Muselaers CH, Oosterwijk E, Hulsbergen-Van de Kaa CA, Boerman
471 OC, et al. Tumor-targeted Dual-modality Imaging to Improve Intraoperative Visualization of Clear Cell
472 Renal Cell Carcinoma: A First in Man Study. Theranostics. 2018;8(8):2161-70.
473 11.   Hekman MCH, Rijpkema M, Bos DL, Oosterwijk E, Goldenberg DM, Mulders PFA, et al.
474 Detection of Micrometastases Using SPECT/Fluorescence Dual-Modality Imaging in a CEA-Expressing
475 Tumor Model. Journal of nuclear medicine : official publication, Society of Nuclear Medicine.
476 2017;58(5):706-10.
477 12.   Tummers WS, Warram JM, van den Berg NS, Miller SE, Swijnenburg RJ, Vahrmeijer AL, et al.
478 Recommendations for reporting on emerging optical imaging agents to promote clinical approval.
479 Theranostics. 2018;8(19):5336-47.
480 13.   Lutje S, Rijpkema M, Helfrich W, Oyen WJ, Boerman OC. Targeted radionuclide and
481 fluorescence dual-modality imaging of cancer: preclinical advances and clinical translation. Molecular
482 imaging and biology : MIB : the official publication of the Academy of Molecular Imaging.
483 2014;16(6):747-55.
484 14.   Lindmo T, Boven E, Cuttitta F, Fedorko J, Bunn PA, Jr. Determination of the immunoreactive
485 fraction of radiolabeled monoclonal antibodies by linear extrapolation to binding at infinite antigen
486 excess. J Immunol Methods. 1984;72(1):77-89.
487 15.   Koppe MJ, Soede AC, Pels W, Oyen WJ, Goldenberg DM, Bleichrodt RP, et al. Experimental
488 radioimmunotherapy of small peritoneal metastases of colorectal origin. International journal of
489 cancer. 2003;106(6):965-72.
490 16.   Rijpkema M, Oyen WJ, Bos D, Franssen GM, Goldenberg DM, Boerman OC. SPECT- and
491 fluorescence image-guided surgery using a dual-labeled carcinoembryonic antigen-targeting
492 antibody. Journal of nuclear medicine : official publication, Society of Nuclear Medicine.
493 2014;55(9):1519-24.
494 17.   Elekonawo FMK, de Gooyer JM, Bos DL, Goldenberg DM, Boerman OC, Brosens LAA, et al. Ex
495 Vivo Assessment of Tumor-Targeting Fluorescent Tracers for Image-Guided Surgery. Cancers (Basel).
496 2020;12(4).
497 18.   Kukis DL, DeNardo GL, DeNardo SJ, Mirick GR, Miers LA, Greiner DP, et al. Effect of the extent
498 of chelate substitution on the immunoreactivity and biodistribution of 2IT-BAT-Lym-1
499 immunoconjugates. Cancer research. 1995;55(4):878-84.
500 19.   Al-Ejeh F, Darby JM, Thierry B, Brown MP. A simplified suite of methods to evaluate chelator
501 conjugation of antibodies: effects on hydrodynamic radius and biodistribution. Nucl Med Biol.
502 2009;36(4):395-402.
503 20.   Lewis MR, Raubitschek A, Shively JE. A facile, water-soluble method for modification of
504 proteins with DOTA. Use of elevated temperature and optimized pH to achieve high specific activity
505 and high chelate stability in radiolabeled immunoconjugates. Bioconjugate chemistry. 1994;5(6):565-
506 76.
507 21.   van Oudheusden TR, Braam HJ, Luyer MD, Wiezer MJ, van Ramshorst B, Nienhuijs SW, et al.
508 Peritoneal cancer patients not suitable for cytoreductive surgery and HIPEC during explorative
509 surgery: risk factors, treatment options, and prognosis. Annals of surgical oncology. 2015;22(4):1236-
510 42.
511 22.   Iversen LH, Rasmussen PC, Laurberg S. Value of laparoscopy before cytoreductive surgery and
512 hyperthermic intraperitoneal chemotherapy for peritoneal carcinomatosis. The British journal of
513 surgery. 2013;100(2):285-92.

514   23.   Pomel C, Appleyard TL, Gouy S, Rouzier R, Elias D. The role of laparoscopy to evaluate
515   candidates for complete cytoreduction of peritoneal carcinomatosis and hyperthermic
516   intraperitoneal chemotherapy. European journal of surgical oncology : the journal of the European
517   Society of Surgical Oncology and the British Association of Surgical Oncology. 2005;31(5):540-3.
518   24.   de Bree E, Koops W, Kroger R, van Ruth S, Witkamp AJ, Zoetmulder FA. Peritoneal
519   carcinomatosis from colorectal or appendiceal origin: correlation of preoperative CT with
520   intraoperative findings and evaluation of interobserver agreement. Journal of surgical oncology.
521   2004;86(2):64-73.
522   25.   Schaap DP, de Valk KS, Deken MM, Meijer RPJ, Burggraaf J, Vahrmeijer AL, et al.
523   Carcinoembryonic antigen-specific, fluorescent image-guided cytoreductive surgery with
524   hyperthermic intraperitoneal chemotherapy for metastatic colorectal cancer. The British journal of
525   surgery. 2020;107(4):334-7.
526   26.   Brouwer NPM, Stijns RCH, Lemmens V, Nagtegaal ID, Beets-Tan RGH, Futterer JJ, et al.
527   Clinical lymph node staging in colorectal cancer; a flip of the coin? European journal of surgical
528   oncology : the journal of the European Society of Surgical Oncology and the British Association of
529   Surgical Oncology. 2018;44(8):1241-6.
530   27.   Boogerd LS, van der Valk MJ, Boonstra MC, Prevoo HA, Hilling DE, van de Velde CJ, et al.
531   Biomarker expression in rectal cancer tissue before and after neoadjuvant therapy. Onco Targets
532   Ther. 2018;11:1655-64.
533   28.   de Gouw D, Rijpkema M, de Bitter TJJ, Baart VM, Sier CFM, Hernot S, et al. Identifying
534   Biomarkers in Lymph Node Metastases of Esophageal Adenocarcinoma for Tumor-Targeted Imaging.
535   Mol Diagn Ther. 2020.
536   29.   van Hagen P, Hulshof MC, van Lanschot JJ, Steyerberg EW, van Berge Henegouwen MI,
537   Wijnhoven BP, et al. Preoperative chemoradiotherapy for esophageal or junctional cancer. The New
538   England journal of medicine. 2012;366(22):2074-84.
539   30.   Vuijk FA, Hilling DE, Mieog JSD, Vahrmeijer AL. Fluorescent-guided surgery for sentinel lymph
540   node detection in gastric cancer and carcinoembryonic antigen targeted fluorescent-guided surgery
541   in colorectal and pancreatic cancer. Journal of surgical oncology. 2018;118(2):315-23.
542   31.   Cuschieri A, Fayers P, Fielding J, Craven J, Bancewicz J, Joypaul V, et al. Postoperative
543   morbidity and mortality after D1 and D2 resections for gastric cancer: preliminary results of the MRC
544   randomised controlled surgical trial. The Surgical Cooperative Group. Lancet (London, England).
545   1996;347(9007):995-9.
546   32.   Bonenkamp JJ, Songun I, Hermans J, Sasako M, Welvaart K, Plukker JT, et al. Randomised
547   comparison of morbidity after D1 and D2 dissection for gastric cancer in 996 Dutch patients. Lancet
548   (London, England). 1995;345(8952):745-8.
549   33.   Hoogstins CES, Boogerd LSF, Sibinga Mulder BG, Mieog JSD, Swijnenburg RJ, van de Velde
550   CJH, et al. Image-Guided Surgery in Patients with Pancreatic Cancer: First Results of a Clinical Trial
551   Using SGM-101, a Novel Carcinoembryonic Antigen-Targeting, Near-Infrared Fluorescent Agent.
552   Annals of surgical oncology. 2018;25(11):3350-7.
553   34.   Hekman MC, Boerman OC, de Weijert M, Bos DL, Oosterwijk E, Langenhuijsen JF, et al.
554   Targeted Dual-Modality Imaging in Renal Cell Carcinoma: An Ex Vivo Kidney Perfusion Study. Clinical
555   cancer research : an official journal of the American Association for Cancer Research.
556   2016;22(18):4634-42.
557   35.   Jay P, Berta P, Blache P. Expression of the carcinoembryonic antigen gene is inhibited by
558   SOX9 in human colon carcinoma cells. Cancer research. 2005;65(6):2193-8.
559   36.   Boonstra MC, de Geus SW, Prevoo HA, Hawinkels LJ, van de Velde CJ, Kuppen PJ, et al.
560   Selecting Targets for Tumor Imaging: An Overview of Cancer-Associated Membrane Proteins.
561   Biomarkers in cancer. 2016;8:119-33.

562

563   Figure 1: Biodistribution of 4 different dose levels of [111 431 In]In-DTPA-SGM-101 in mice (n= 5 per

564   dose level) with subcutaneous LS174T tumors. 1 group received a dose with an excess of 1 mg of

565   unlabeled DTPA-SGM-101 as control group (gray, n= 5).

566   Figure 2: SPECT/CT imaging shows extensive metastatic disease within the abdominal cavity in a

567   mouse with intraperitoneally induced tumors (A). After surgical exposure several tumor deposits are

568   visible (B). Fluorescence imaging shows that after resection of macroscopically visible lesions several

569   tumor deposits remain present within the abdominal cavity (C/D). After fluorescence-guided

570   resection is performed, no additional lesions are visible within the abdominal cavity and only

571   physiological uptake of the tracer in the liver remains (E).

572   Figure 3: Fluorescence-based (green, top graph) and radiosignal based (blue, bottom graph) tumor to

573   background ratios after incubation of surgically obtained tissue specimens. Tumor deposits from case

574   9 and 10 were cut in half, each corresponding half was incubated with [^{111}In]In-DTPA-SGM-101 (9* &

575   10*) or aspecific [^{111}In]In-DTPA-IgG-Cy5.5 (9** & 10**). Case 7 was a CEA-negative malignancy

576   (LAMN). Average tumor to background ratios are shown in orange.

577   Figure 4: Three examples of slides from the ex vivo incubation experiment on human tissues. From

578   left to right: H&E staining, CEA staining, NIR-fluorescence and autoradiography. Clear co-localization

579   of CEA-expressing tumor cells and both fluorescence and radiosignal is observed.
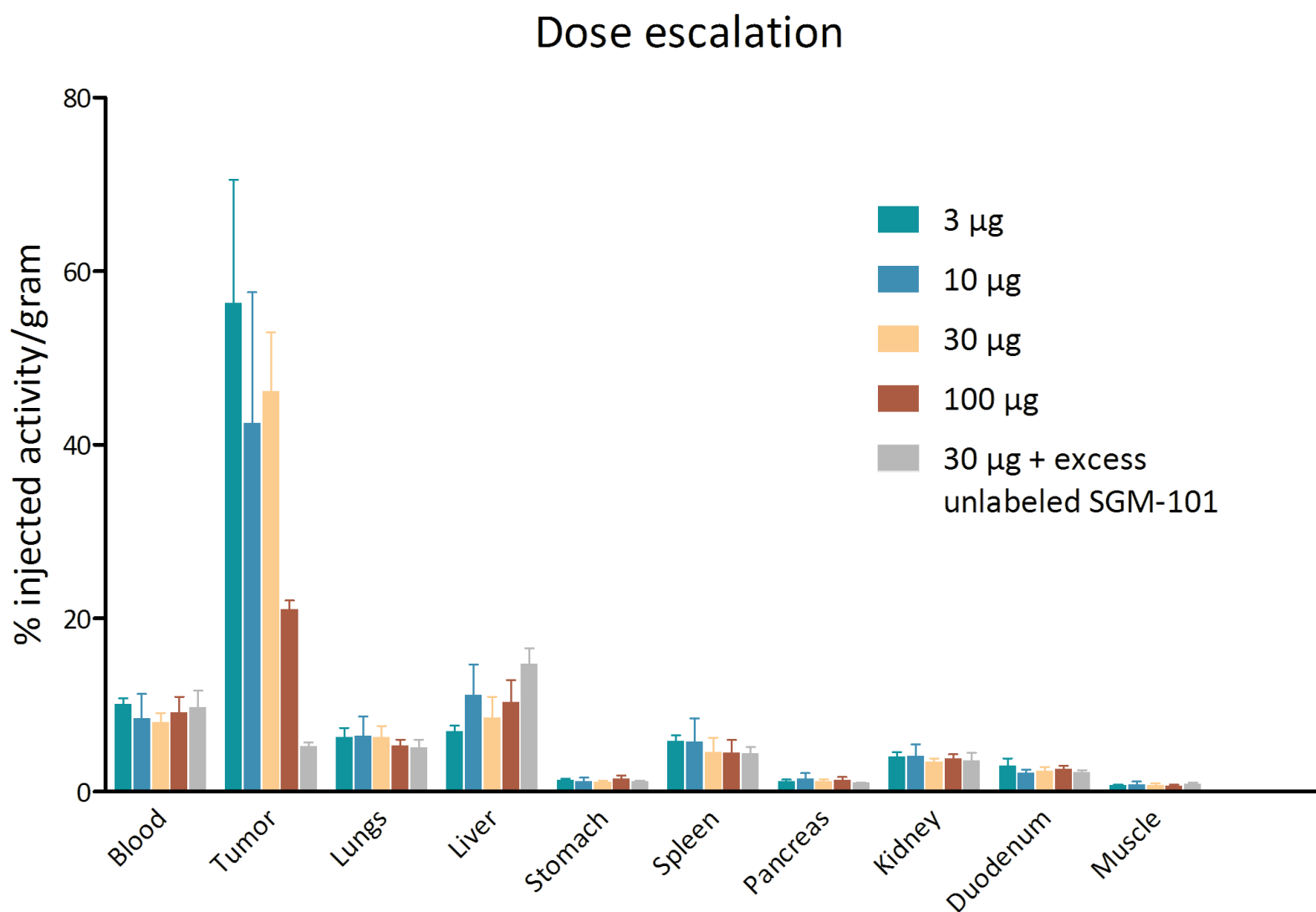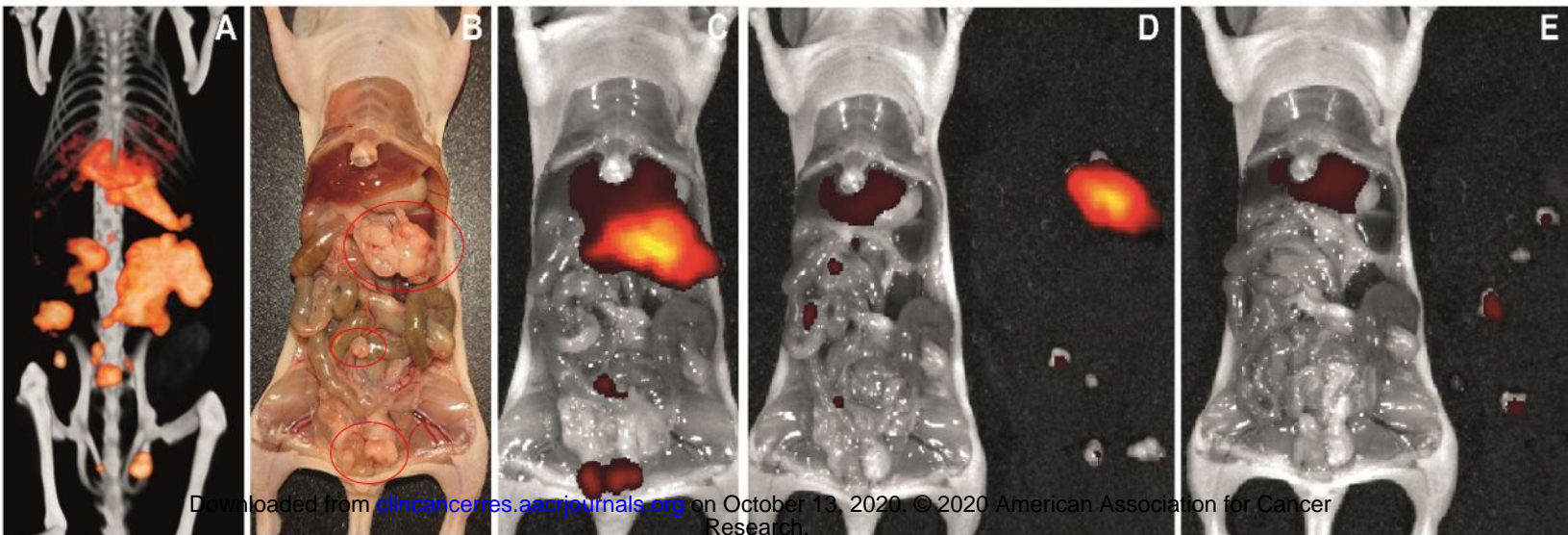
Figure 1

Dose escalation

Figure 2

Figure 3

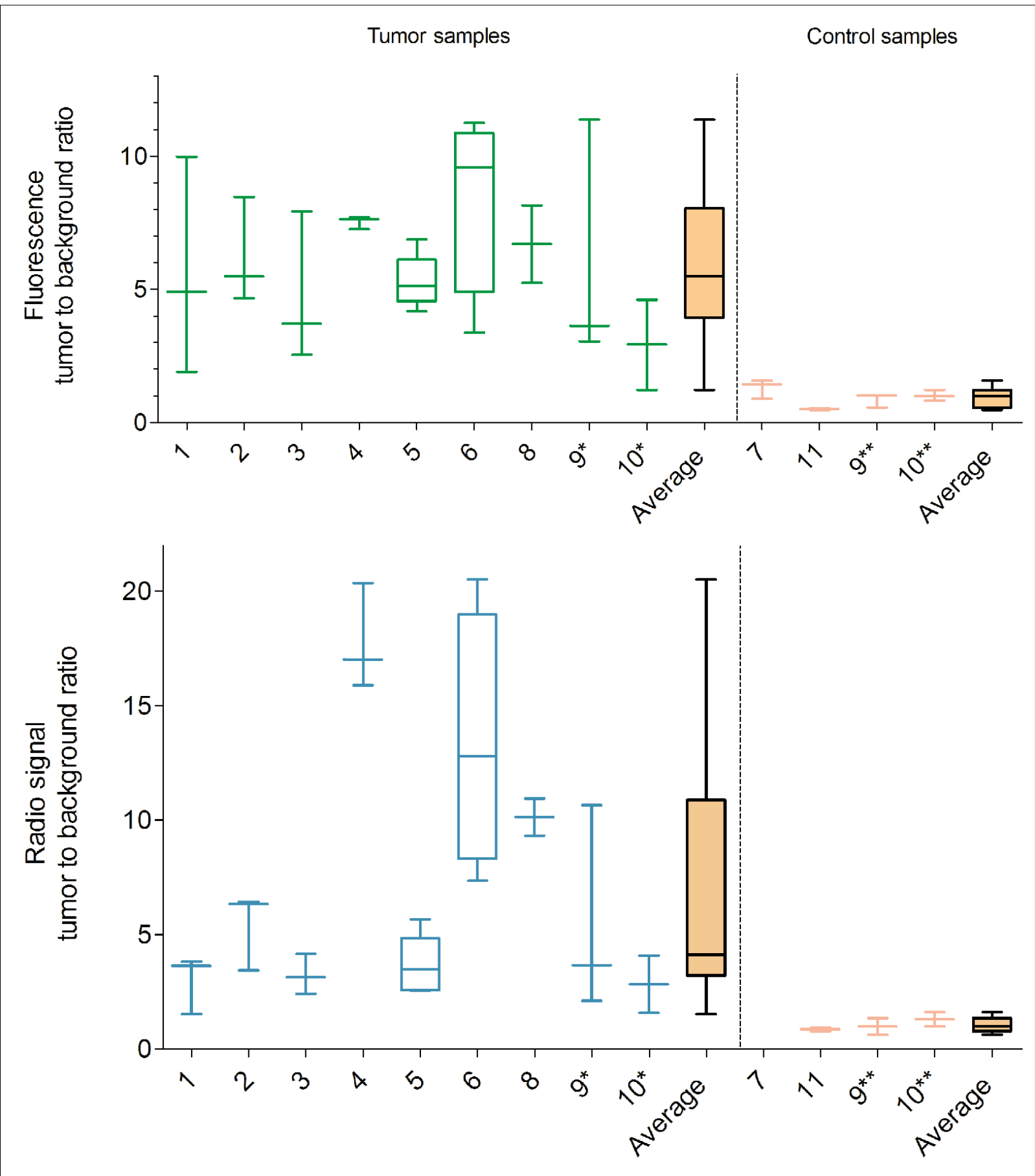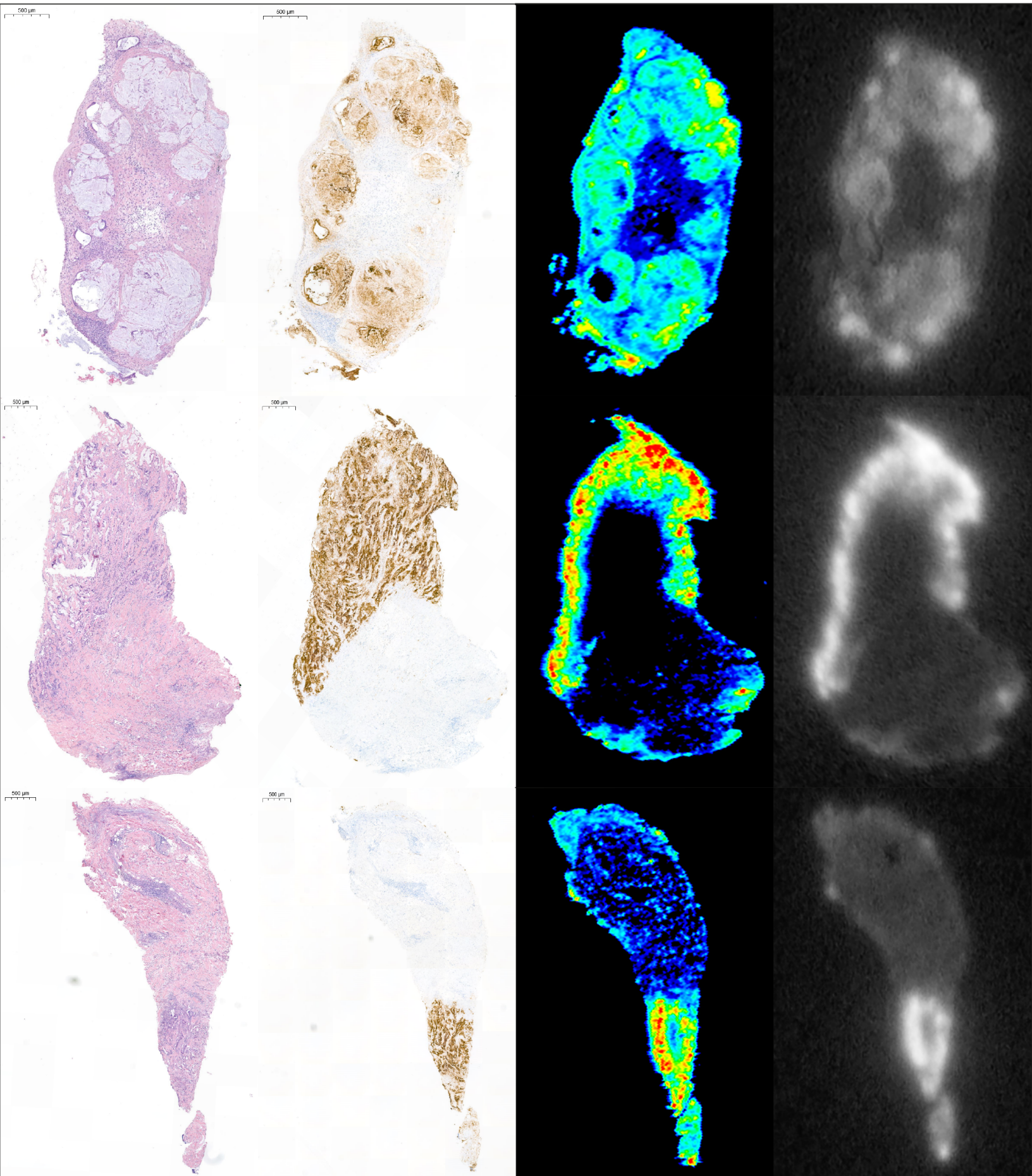Figure 4

AAGR American Association for Cancer Research

Clinical Cancer Research

Multimodal CEA-targeted image-guided colorectal cancer surgery using 111In-labeled SGM-101

Jan Marie de Gooyer, Fortuné M.K. Elekonawo, Desirée L. Bos, et al.

Updated version	Access the most recent version of this article at: doi:10.1158/1078-0432.CCR-20-2255
Supplementary Material	Access the most recent supplemental material at: http://clincancerres.aacrjournals.org/content/suppl/2020/09/30/1078-0432.CCR-20-2255.DC1
Author Manuscript	Author manuscripts have been peer reviewed and accepted for publication but have not yet been edited.

E-mail alerts	Sign up to receive free email-alerts related to this article or journal.
Reprints and Subscriptions	To order reprints of this article or to subscribe to the journal, contact the AACR Publications Department at pubs@aacr.org.
Permissions	To request permission to re-use all or part of this article, use this link http://clincancerres.aacrjournals.org/content/early/2020/09/05/1078-0432.CCR-20-2255. Click on "Request Permissions" which will take you to the Copyright Clearance Center's (CCC) Rightslink site.